Rapidly contracting subdivision yields finite, effectively C^2 surfaces

Kęstutis Karčiauskas and Jörg Peters

August 24, 2018

Abstract

Tools of subdivision theory allow constructing surfaces that are effectively C^2 and have a good highlight line distribution also near irregularities where more or fewer than four quadrilateral patches meet. Here, effectively C^2 means that transitions that are only first-order smooth are confined to a tiny multi-sided cap. The cap can be chosen smaller than any refinement required for geometric modeling or computing on surfaces. The remainder of the surface parameterization is C^2. The resulting surface is of degree bi-5 and consists of three or fewer surface rings that are rapidly converging towards the tiny central cap.

keywords: rapid contraction, subdivision, C2 surface, good highlight line distribution, total degree guide surface

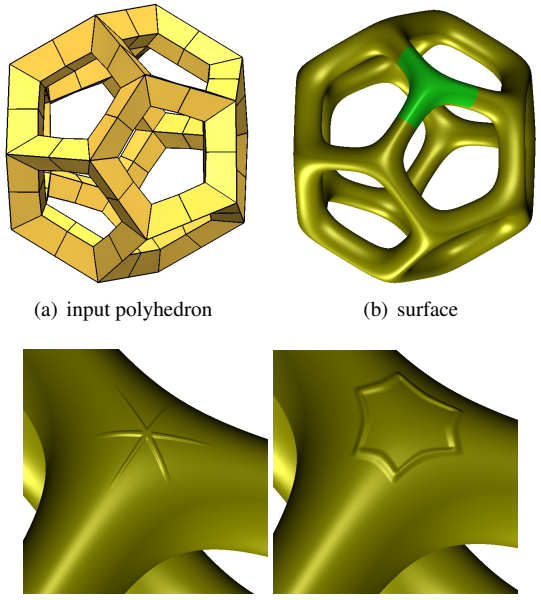

(a) input polyhedron (b) surface

(c) embossed fine features

Figure 1: Rapid, effectively C^2 surfaces offer modeling and analysis at several scales. Although subdivision-based, they can be treated as surfaces with finitely many patches: the green piece in (b) consists of three bi-5 C^2-connected rings plus a tiny G^1 bi-5 cap. Fig. 19 shows additional detail.

1 Introduction

Classical subdivision algorithms, such as Catmull-Clark subdivision or Doo-Sabin subdivision [1, 2] appeal to artists due to their simple local refinement rules that cut the edges of an initial polyhedron to arrive at a smooth limit surface. Another property that is useful when computing, say physical fields, on the resulting surfaces is that patches join with a fixed re-parameterization, namely the identity between pieces of the same subdivision level; and a binary scaling between pieces of the next finer level at the T-joints between subdivision rings. But the simplicity of the construction comes at a price: subdivision surfaces are known to have artifacts [3, 4] that prevent their use for class A styling design (see e.g. [5, 6] for early work to improve shape.) Also practitioners that have to deal with the surfaces downstream complain about the large num-

ber of polynomial pieces. While the number of nested subdivision surface rings is theoretically infinite, in practice refinement is stopped at a level that requires extreme enlargement if one wanted to notice the remaining tiny hole that would be filled by the infinite sequence of subdivision rings. The hole may then simply be triangulated. Yet, the number of refinements in practice often reaches six or more, taxing downstream operations.

It is therefore tempting, and in line with actual practice, to replace pure subdivision with a hybrid construction that switches after a few steps to a finite, geometrically continuous surface cap. Recent constructions, such as [7, 8] blur the line between subdivision surfaces and such finite G^1 surfaces.

We improve on these approaches by accelerating the subdivision to require fewer subdivision rings. In place of six rings, three or fewer achieve sufficient contraction, even for high valences. The key to such rapid subdivision is a characteristic subdivision map (see e.g. [9, Ch. 5]) with accelerated contraction [10]. Notably, the new hybrid construction is stabilized by referencing a guide surface, an idea proposed in [6]. (The guide of the new construction differs however considerably from [6]: it is C^1 with a unique cubic expansion at the center point instead of C^2 with a unique quadratic expansion.)

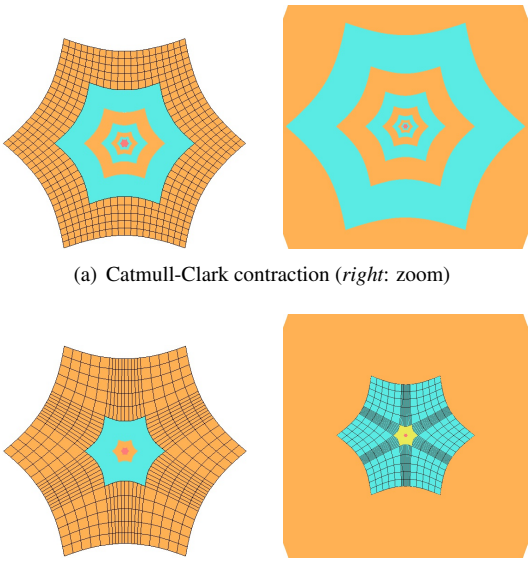

(a) Catmull-Clark contraction (*right*: zoom)

(b) rapid contraction (*right*: zoom)

Figure 2: The contraction of (a) two steps at the speed of Catmull-Clark subdivision approximately equals that of (b) one rapid subdivision step. The center is filled with a tiny red G^1 surface cap.

2 Definitions and Setup

2.1 A B-spline-like control net for irregular layout

We consider as input a network of quadrilateral facets, short quads. Nodes where four quads meet are regular, else *irregular*. We assume that each irregular node is surrounded by at least one layer of regular nodes, i.e. the all other nodes of the quads meeting at the irregular node are regular. Fig. 3a shows the $\mathbf{c}$-net (bullets) of an isolated node of valence $n = 5$. The $\mathbf{c}$-net consists of the irregular node plus $6n$ nodes forming two layers of quads surrounding it. Typically a third layer is added for evaluation of local shape (yielding the green surface in Fig. 3b). This allows assessing the highlight line distribution [11] across the transition which is as important as the internal quality of the cap.

Each 4×4 sub-grid of nodes is interpreted as the B-spline control points of a bicubic tensor-product spline surface. Except at the irregular node, well-known formulas can be applied to convert the B-spline form to Bernstein-Bézier form (see e.g. [12, 13]). The tensor-product Bernstein-Bézier (BB) form of bi-degree d is

$$\mathbf{p}(u,v) := \sum_{i=0}^{d}\sum_{j=0}^{d} \mathbf{p}_{ij} B_i^d(u) B_j^d(v) \,,$$

$$(u,v) \in \square := [0..1]^2, \qquad \text{where } B_k^d(t) := \binom{d}{k}(1-t)^{d-k}t^k$$

are the BB-polynomials of degree d and $\mathbf{p}_{ij}$ are the BB coefficients. Fig. 3b also shows the C^2 prolongation of this surface ring, i.e. Hermite data represented as a grid (black) of bi-3 BB-coefficients. Specifically, the BB-coefficients $\mathbf{p}_{ij}$, $i = 0,\ldots,3$, $j = 0,\ldots,2$, represent Hermite data of order 2 along one boundary curve $v = 0$. We call these data $\mathbf{t}_{CC}$. More generally, in the remainder of this paper, we refer to second-order Hermite data of degree 5 along the loop of boundary curves as $\mathbf{t}$.

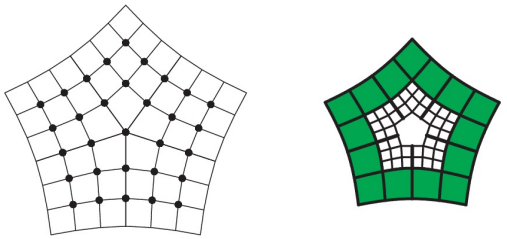

(a) **c**-net extended by 1 layer (b) bi-3 ring + tensor-border

Figure 3: B-spline-like irregular control net and its tensor-border. (a) Extended **c**-net for $n = 5$. (b) Schema of surface ring (green) and its tensor-border (mesh of BB-coefficients) of degree 3 and depth 2. The tensor-border is the input for the surface construction.

2.2 Corner jet constructor $[f]$

We will construct tensor-product patches and tensor-borders with a help of *corner jet constructor* $[f]$ that expresses, at a corner of the domain square $[0..1]^2$, the expansion of function f order 2 in both u and v directions in BB-form of bi-degree 5. That is, $[f]$ outputs 3×3 BB-coefficients (see Fig. 4a,b). Fig. 4c displays four corner jet constructors merged to form a bi-5 patch while Fig. 4d illustrates the analogous assembly of an L-shaped sector of the tensor-border by applying a jet constructor at three corners.

Several steps of the surface construction enforce a simple linear relationship, called C2-rule: two curve segments (of the same degree) in BB-form join C^2 at their common end-point (marked as a big bullet) if and only if the BB-coefficient immediately its *left* (small circle indicated by $\downarrow$ in Fig. 5) is defined as the weighted average of the BB-coefficients marked as bullets with the weights indicated above. The *right* circled BB-coefficient in Fig. 5 is defined by the mirrored formula.

3 A guide surface g of total degree 6

The domain of the map $\mathbf{b}^{\triangle}$ of total degree d is a regular n-gon D composed from n equal triangles with a common vertex $\mathbf{O}$ at the origin. Fig. 6a shows one such triangle with sides defined by $l_i = 0$, $i = 0, 1, 2$. Each linear function l_i is equal to 1 at the vertex opposite to $l_i = 0$.

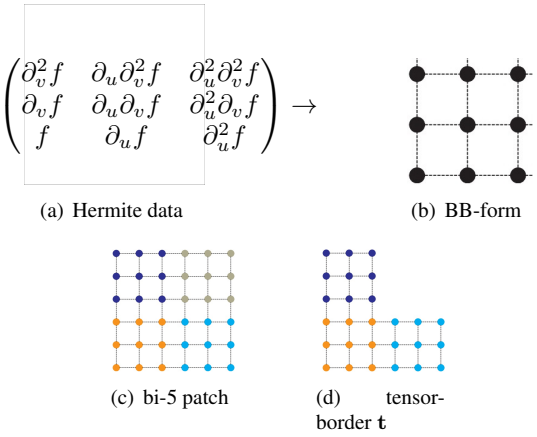

(a) Hermite data (b) BB-form

(c) bi-5 patch (d) tensor-border $\mathbf{t}$

Figure 4: (a) Hermite data as partial derivatives converted to (b) BB-form; (c) a patch of degree bi-5; (d) the L-shaped sector of the tensor-border $\mathbf{t}$.

Figure 5: Symmetric rule of C^2 join.

On the triangle we define a map $\mathbf{b}$ of *total degree* d in Bernstein-Bézier form as

$$\mathbf{b} := \sum_{i+j+k=d} \mathbf{b}_{ijk} B^d_{ijk}, \; i,j,k \geq 0, \quad B^d_{ijk} := \binom{d}{ijk} l_0^i l_1^j l_2^k . \tag{1}$$

Fig. 6b labels the BB-coefficients rotationally symmetric. Let

$$\mathsf{c} := \cos \frac{2\pi}{n}, \quad w_0 := -1, \; w_1 := 2\mathsf{c}, \; w_2 := 2(1 - \mathsf{c}).$$

Pieces on adjacent sectors $\mathbf{b}^s$ and $\mathbf{b}^{s+1}$ join

$$C^0 \text{ if } \quad \mathbf{b}^{s+1}_{d-i,i,0} := \mathbf{b}^s_{d-i,0,i}, \quad i=0,\ldots,d \tag{2}$$

$$C^1 \text{ if } \quad \mathbf{b}^{s+1}_{d-i,i-1,1} := w_0\mathbf{b}^s_{d-i,1,i-1} + w_1\mathbf{b}^s_{d-i,0,i} + w_2\mathbf{b}^s_{d-i+1,0,i-1}, \quad i=1,\ldots,d \tag{3}$$

$$C^2 \text{ if } \quad \mathbf{b}^{s+1}_{d-i,i-2,2} := w_0^2\mathbf{b}^s_{d-i,2,i-2} + 2w_0w_1\mathbf{b}^s_{d-i,1,i-1} + w_1^2\mathbf{b}^s_{d-i,0,i} + 2w_0w_2\mathbf{b}^s_{d-i+1,1,i-2} + 2w_1w_2\mathbf{b}^s_{d-i+1,0,i-1} + w_2^2\mathbf{b}^s_{d-i+2,0,i-2}, \quad i=2,\ldots,d. \tag{4}$$

$$C^3 \text{ if } \quad \mathbf{b}^{s+1}_{d-i,i-3,3} := w_0^3\mathbf{b}^s_{d-i,3,i-3} + 3w_0^2w_1\mathbf{b}^s_{d-i,2,i-2} + 3w_0w_1^2\mathbf{b}^s_{d-i,1,i-1} + w_1^3\mathbf{b}^s_{d-i,0,i} + 3w_0^2w_2\mathbf{b}^s_{d-i+1,2,i-3} + 6w_0w_1w_2\mathbf{b}^s_{d-i+1,1,i-2} + 3w_1^2w_2\mathbf{b}^s_{d-i+1,0,i-1} + 3w_0w_2^2\mathbf{b}^s_{d-i+2,1,i-3} + 3w_1w_2^2\mathbf{b}^s_{d-i+2,0,i-2} + w_2^3\mathbf{b}^s_{d-i+3,0,i-3}, \quad i=3,\ldots,d. \tag{5}$$

across the *sector boundary* between patch s and patch $s+1$ (modulo n). In the following,
– superscript s denotes the sector, i.e. $s \in \{0,1,\ldots,n-1\}$ and
– superscript r denotes the refinement level, i.e. $r = 0,1,\ldots$.
The ten BB-coefficients $\mathbf{b}^0_{ijk}$ (indicated as red bullets in Fig. 6) define a cubic expansion $\mathbf{q}$ at the central point $\mathbf{b}^0_{d00}$. This local expansion is propagated to the neighboring sectors by repeatedly enforcing Eq. (2) for $i = 0,1,2,3$, Eq. (3) for $i = 1,2,3$ and Eq. (4) for $i = 2,3$ and Eq. (5) for $i = 3$. That is, the $\mathbf{b}^0_{ijk}$ define a unique cubic expansion of the C^1 map $\mathbf{b}^\triangle$ at $\mathbf{b}^0_{d00}$.

With the cubic expansion fixed, the C^1 constraints (3) can be rewritten as

$$\mathbf{b}^s_{d-i,0,i} := \frac{1}{2\mathsf{c}}\left(\mathbf{b}^s_{d-i,1,i-1} + \mathbf{b}^{s+1}_{d-i,i-1,1}\right) + (1-\frac{1}{\mathsf{c}})\mathbf{b}^s_{d-i+1,0,i-1}, \quad i=4,\ldots,d. \tag{3'}$$

leaving the BB-coefficients

$$\mathbf{b}^s_{213}, \mathbf{b}^{s+1}_{231}, \mathbf{b}^s_{114}, \mathbf{b}^{s+1}_{141}, \mathbf{b}^s_{015}, \mathbf{b}^{s+1}_{051}$$

of $\mathbf{b}^\triangle$ unrestricted by the C^1 continuity constraints (see Fig. 6b; coefficients unrestricted due to their distances from the sector boundary are underlaid gold).

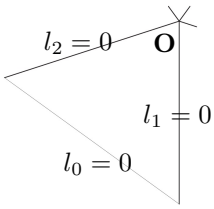

(a) domain

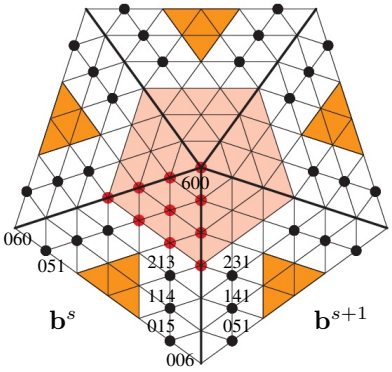

(b) $\mathbf{b}^\triangle$

Figure 6: (a) Domain of total degree d map. (b) The $n = 5$ sectors of the C^1 map $\mathbf{b}^\triangle$ of total degree 6. The coefficients of the cubic expansion at the center are underlaid light red. BB-coefficients unrestricted after enforcing the C^1 constraints are marked as black and red bullets. The gold underlaid BB-coefficients do not affect C^1 continuity between sectors.

The resulting map $\mathbf{b}^\triangle$ is a piecewise C^1 map of total degree 6 with a unique cubic expansion at the central point and $12n + 10$ free parameters: 10 defining the cubic expansion, $6n$ marked as black bullets and $6n$ gold-underlaid in Fig. 6. When serving as a guide surface, we will denote the piecewise C^1 map by $\mathbf{g}$.

4 Bi-5 guided subdivision

4.1 Rapid characteristic parameterizations χ_σ and $\tilde{\chi}_\sigma$

The subdominant eigenvalue of bi-3 adjustable speed subdivision [10] with 'speed' parameter σ is

$$\lambda_\sigma := \frac{\tilde{\sigma}}{2}((1+\mathsf{c})\sigma^2 + 2\tilde{\sigma} + \sigma\sqrt{(1+\mathsf{c})((1+\mathsf{c})\sigma^2 + 4\tilde{\sigma})}),$$
$$\tilde{\sigma} := 1-\sigma, \quad 0<\sigma<1.$$

When $\sigma := \frac{1}{2}$ then λ_σ is the subdominant eigenvalue of Catmull-Clark subdivision, $\sigma > \frac{1}{2}$ yields faster and $\sigma < \frac{1}{2}$ yields slower contraction. Already for $\sigma \approx \frac{1}{2}$, analogous to Catmull-Clark subdivision, the subdivision surfaces of [10] do not qualify for high-end design; and the shape deteriorates with increasing σ.

Fig. 7*top* displays, for $n = 5$ and one sector, several characteristic maps χ_σ Fig. 7*bottom* displays the corresponding characteristic tensor-borders $\tilde{\chi}_\sigma$ of degree 3 and depth 2. In the classical analysis of Catmull-Clark subdivision these tensor-borders are hidden as the maps χ_σ contain the key analytic information, while for construction of rapid subdivision these C^2 prolongations are in the forefront. The gray underlaid BB-coefficients of χ_σ are the result of splitting $\tilde{\chi}_\sigma$ in the ratio $\sigma : 1-\sigma$ (see Fig. 7b). Clearly different σ result in different maps, according to the speed. By contrast the (normalized) corresponding tensor-borders $\tilde{\chi}_\sigma$ in Fig. 7d,e,f look almost identical. This explains why we do not observe artifacts when switching from one choice of σ to another in consecutive subdivision steps.

4.2 Determining the guide g

In particular, we form the contracting bi-5 guided subdivision rings from tensor-borders $\mathbf{t}$ (see Fig. 8b) assembled, as in Fig. 4d, from corner jets

$$[\mathbf{g} \circ (\mu\, \tilde{\chi}_\sigma)], \quad \text{for } 0<\mu<1 \tag{6}$$

that sample $\mathbf{g}$ in each sector at the locations marked as crosses in Fig. 8a. The sectors of $\mathbf{t}$ are automatically C^1-connected and applying the C2-rule C^2-connects the updated sectors of $\tilde{\mathbf{t}}$ shown in Fig. 8c. Fig. 8a juxtaposes $\tilde{\chi}_\sigma$ and its scaled copy $\mu\tilde{\chi}_\sigma$. Specifically, we initialize the

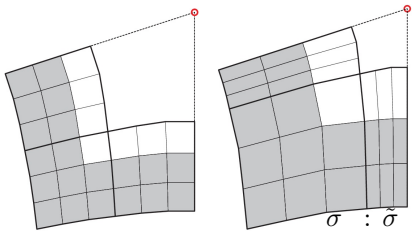

(a) $\sigma := \frac{1}{2}$ (CC) (b) $\sigma := \frac{3}{4}$

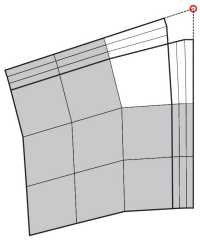

(c) $\sigma := \frac{7}{8}$

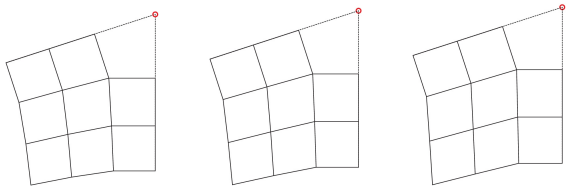

(d) $\sigma := \frac{1}{2}$ (CC) (e) $\sigma := \frac{3}{4}$ (f) $\sigma := \frac{7}{8}$

Figure 7: (*top row*) χ_σ; (*bottom row*) $\tilde{\chi}_\sigma$.

guide using $\sigma := \frac{1}{2}$ and set, in terms of the $\mathbf{c}$-net nodes $\mathbf{c}_i^k$ (see Fig. 9, $\mathbf{c}_7^k$, $k = 0,\ldots,n-1$, is the central node), the central BB-coefficient $\mathbf{b}_{600}^0$ to

$$\text{if } n>4, \quad \frac{n}{n+5}\mathbf{c}_7^0 + \sum_{k=0}^{n-1}(\gamma_5\mathbf{c}_5^k + \gamma_6\mathbf{c}_6^k), \tag{7}$$
$$\gamma_5 := \frac{1}{n(n+5)}, \quad \gamma_6 := 4\gamma_5,$$

$$\text{if } n=3, \quad (1-3\gamma_5-3\gamma_6)\mathbf{c}_7^0 + \sum_{k=0}^{2}(\gamma_5\mathbf{c}_5^k + \gamma_6\mathbf{c}_6^k), \tag{8}$$
$$\gamma_5 := \frac{5}{96},\ \gamma_6 := \frac{1}{6},$$

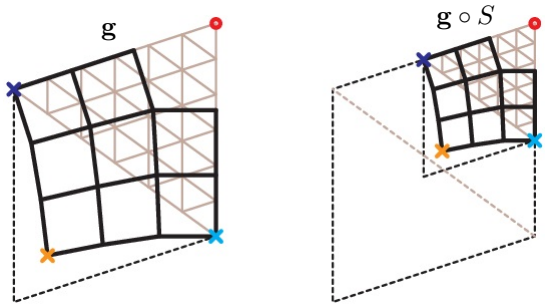

(a) scaled sampling

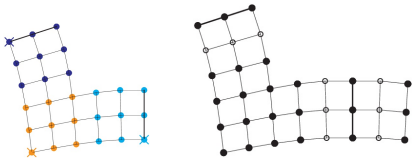

(b) $\mathbf{t}$ (c) $\tilde{\mathbf{t}}$

Figure 8: (a) Map $\tilde{\chi}_\sigma$ for sampling the guide $\mathbf{g}$; (b) sampled C^1 tensor-border $\mathbf{t}$; (c) upgrade from C^1 $\mathbf{t}$ to C^2 $\tilde{\mathbf{t}}$.

i.e. as the extraordinary point of Catmull-Clark subdivision except for a small perturbation to improve shape when $n = 3$. The remaining set Γ of $12n + 9$ free parameters is fixed by minimizing the sum of squared distances between corresponding control points of the input tensor-border $\mathbf{t}_{CC}$ degree-raised to 5 and the tensor-border $\mathbf{t}$ assembled from corner jets $[\mathbf{g} \circ \tilde{\chi}_\sigma]$ (that depend linearly on Γ via (6)). In short, the $\mathbf{c}$-net fully determines $\mathbf{g}$.

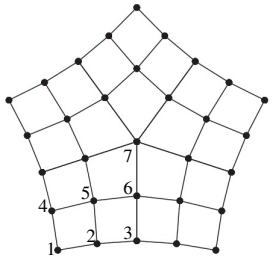

Figure 9: Rotationally-symmetric labelling of the $\mathbf{c}$-net nodes $\mathbf{c}_m^k$, $m = 1, \ldots, 7$ of one sector k.

Implementation of g via generating functions The initialization works for each coordinate separately. When all nodes of $\mathbf{c}$-net have value 0, except that $\mathbf{c}_m^0 = 1$ for one of $m = 1, \ldots, 7$ (see Fig. 9), we obtain the 28 scalar-valued total degree 6 coefficients

$$h_i^{k,m} \in \mathbb{R},\ k = 0, \ldots, n-1,\ m = 1, \ldots, 7,\ i = 1, \ldots, 28,$$

where $h_i^{0,7} = \ldots = h_i^{n-1,7}$. Then the BB-coefficients of sector s of $\mathbf{g}$ are

$$\mathbf{g}_i^s := h_i^{0,7}\mathbf{c}_7^0 + \sum_{k=0}^{n-1}\sum_{m=1}^{6} h_i^{k,m}\mathbf{c}_m^{s-k}\ ,$$

where the superscript of $\mathbf{c}_m^{s-k}$ is interpreted modulo n.

Repeated sampling of contracted guide Computing $[\mathbf{g} \circ (\mu\tilde{\chi}_\sigma)]$ is equivalent to linearly mapping $S : D \to \mu D$ and sampling $(\mathbf{g} \circ S) \circ \tilde{\chi}_\sigma$. DeCasteljau's algorithm (see Appendix) yields the BB-coefficients of $\mathbf{g} \circ S$ as affine combinations of the BB-coefficients of $\mathbf{g}$. Due to combinatorial symmetry of the construction we need only precompute one 28×28 matrix for de Casteljau refinement and, per σ (typically $\sigma \in \{\frac{3}{4}, \frac{7}{8}, \frac{15}{16}\}$), one 27×28 matrix for the BB-coefficients of $\tilde{\mathbf{t}}$. Taking in to account that the sampled tensor-border $\mathbf{t}$ is automatically C^1 and the updated tensor-border $\tilde{\mathbf{t}}$ joins sectors C^2 (see Fig. 8c) we only need to store an 18×28 matrix per σ.

4.3 Construction of bi-5 rings

With superscripts denoting the refinement level (scaling) of the ring, the **Construction Algorithm** is as follows.

- Choose the maximal anticipated refinement level ℓ and the sequence of speeds σ_r, $r = 1, \ldots, \ell$. The default is $(\sigma_1, \sigma_2, \sigma_3) := (\frac{3}{4}, \frac{7}{8}, \frac{7}{8})$.
- Initialize $\mathbf{g}^0 := \mathbf{g}$ and $\tilde{\mathbf{t}}^0$ as $\mathbf{t}_{CC}$ degree-raised to 5.
- Per sector, apply the (pre-computed) deCasteljau split with $\mu := \lambda_{\sigma_r}$ to obtain the BB-coefficients of $\mathbf{g}^r$ from $\mathbf{g}^{r-1}$.
- Applying the pre-computed sampling formulas to $\mathbf{g}^r \circ \sigma_r$ followed by C2-rule-upgrade yields $\tilde{\mathbf{t}}^r$.
- Split $\tilde{\mathbf{t}}^{r-1}$ in the ratio $\sigma_r : \tilde{\sigma}_r$ to define the outer three layers of BB-coefficients of the three bi-5 patches of a sector (dark-gray underlaid in Fig. 10).

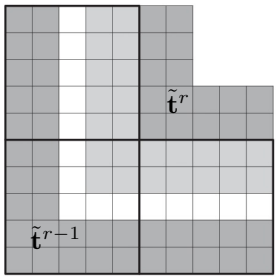

(a) $\sigma_r = \frac{1}{2}$

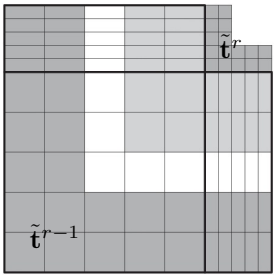

(b) $\sigma_r = \frac{3}{4}$

Figure 10: Merging the tensor-borders $\tilde{\mathbf{t}}^{r-1}$ and $\tilde{\mathbf{t}}^r$ to form a bi-5 ring (for comparison two different σ_r cases are shown).

- Choose the inner (closer to the center) BB-coefficients of $\mathbf{x}^{r-1}$ (light-gray underlaid in Fig. 10) as a C^2 prolongation of $\tilde{\mathbf{t}}^r$.

Due to the last step, consecutive rings join C^2.

5 The eigen-structure of guided bi-5 subdivision limit surfaces

While, for applications, a few steps of rapid subdivision typically suffice, a complete theoretical analysis of the subdivision limit surface is possible.

5.1 The guide g as a superposition of homogeneous functions

Since the Bernstein polynomials $B^d_{0jk} := \binom{d}{0jk} l_1^j l_2^k$ are homogeneous of degree d, $B^d_{0jk}(\lambda x) = \lambda^d B^d_{0jk}(x)$ for any λ. The homogeneity is not affected by constraints (2-5). If we set one unconstrained BB-coefficient to 1 and the others to 0, the resulting $\mathbf{g}$ is homogeneous in all sectors. These simple observations yield an efficient explicit decomposition of the guide $\mathbf{g}$ into homogeneous functions. We count

- 10 functions corresponding to cubic expansion: the function 1, two linear functions of degree 1, three of degree 2 and four of degree 3.

- $6n$ functions that are non-zero on two adjacent sectors: $2n$ of degree 4, $2n$ of degree 5 and $2n$ of degree 6.

- $6n$ functions (n groups of 6) that are non-zero only in one sector: B^4_{022} of degree 4, B^5_{032}, B^5_{023} of degree 5, B^6_{042}, B^6_{033}, B^6_{024} of degree 6.

5.2 The eigen-structure of guided subdivision surfaces

If all $\sigma_r = \sigma$, the bi-5 guided subdivision surfaces inherit the homogeneous decomposition of the guide $\mathbf{g}$. For analyzing the eigenstructure, we denote as $\mathbf{x}^0$ the first ring using the final fixed constant σ, and by $\mathbf{x}^r_{d,p}$ the rth ring obtained applying the Construction Algorithm to the pth homogeneous function $\mathbf{f}_{d,p}$ of degree d of Section 5.1. Then $\mathbf{x}^r_{d,p} = (\lambda^d_\sigma)^r \mathbf{x}^0_{d,p}$. (This implies that we can, analogous to [14], pre-compute the initial $12n+10$ eigen-rings $\mathbf{x}^0_{d,p}$ and compute eigen-functions $\mathbf{x}^r_{d,p}$ simply by scaling by $(\lambda^d_\sigma)^r$. Since homogeneous functions are closely related to monomials of the power form, it is clear that they serve subdivision analysis whereas the BB-form should be used for modelling.)

Smoothness at the extraordinary point The linear combination of the two homogeneous eigen-functions of degree 1 re-produce χ_σ. Since χ_σ is injective [10], the eigen-spectrum of $\mathbf{g}$ implies that the bi-5 guided subdivision surfaces are generically at least C^1 and curvature-bounded.

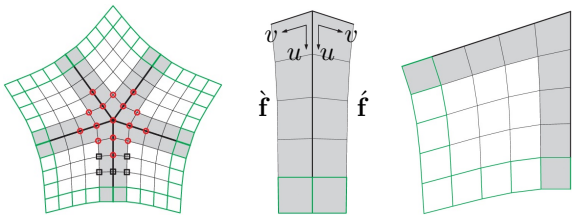

(a) bi-5 cap (b) G^1 (c) τ

Figure 11: (a) The structure of the bi-5 cap. (b) G^1 constraints. (c) The parameterization τ.

6 The central cap

The central cap $\mathbf{p}$ is formed by n G^1-connected bi-5 patches that join C^1 with the last ring $\mathbf{x}^{\ell-1}$. The C^1 prolongation of $\mathbf{x}^{\ell-1}$ defines the green underlaid BB-coefficients of $\mathbf{p}$ in Fig. 11a. The light-gray underlaid BB-coefficients enforce

$$\partial \grave{\mathbf{f}}_v + \partial \acute{\mathbf{f}}_v - 2\mathsf{c}(1-u)^2 \partial \grave{\mathbf{f}}_u = 0, \tag{9}$$

symmetric G^1 constraints between the adjacent patches (see Fig. 11b).

Planar reparameterization τ First, for (each) fixed σ we construct a symmetric planar parameterization τ (Fig. 11c shows one sector when $n = 5$) so that

- the adjacent sectors of τ satisfy the constraints (9);
- the BB-coefficients that are green underlaid in Fig. 11c stem from $\tilde{\chi}_\sigma$ degree-raised to degree bi-5;
- τ is rotationally symmetric and symmetric with respect to the sector-diagonal.

Then τ has 7 remaining parameters that we abbreviate Γ and determine by minimizing

$$\min_{\Gamma} \sum_{s=0}^{n-1,*} \mathcal{F}_5(\tau^s), \quad \mathcal{F}_k f := \int_0^1 \int_0^1 \sum_{\substack{i+j=k \\ i,j\geq 0}} \frac{k!}{i!j!} (\partial_s^i \partial_t^j f)^2 ds dt, \tag{10}$$

where * indicates that the sum is over both coordinates of τ. Due to symmetry, this minimization is local to one sector.

The subsequent calculations work with symbolic coefficients of $\mathbf{g}$ to obtain a general formula in terms of any geometric realization of the guide $\mathbf{g}$.

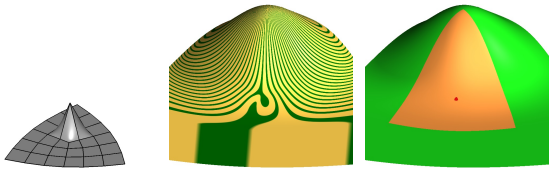

(a) $n = 3$ c-net (b) Catmull-Clark (c) layout

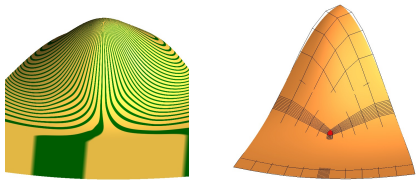

(d) highlight lines (e) 'rapid' BB-net

Figure 12: Valence $n = 3$ and choice $\ell = 1$, $\sigma = (\frac{15}{16})$. The central cap is red.

- Assemble a map $\mathbf{a}$ from corner jets $[\mathbf{g} \circ \tau]$ as in Fig. 4. (The red BB-coefficients f $\mathbf{a}$ at the center are then consistent with the G^1 constraints (9).)
- Replace the green underlaid BB-coefficients of $\mathbf{a}$ with those of the tensor-border $\tilde{\mathbf{t}}$.
- Enforce the G^1 constraints (9) along the sector separators by expressing the five BB-coefficients marked by black squares in Fig. 11a as an affine combinations of the local tensor-border, the quadratic expansion and two free BB-coefficients.
- Set the two free BB-coefficients by minimizing the sum of squared distances between the five square BB-coefficients and their counterparts in $\mathbf{a}$.

The resulting formulas are applied to $\mathbf{g}^\ell$ and $\tilde{\mathbf{t}}^\ell$. Since the red BB-coefficients in Fig. 11a represent a reparameterized quadratic expansion of $\mathbf{g}^\ell$ at the extraordinary point, the G^1 cap has well-defined curvature at the center.

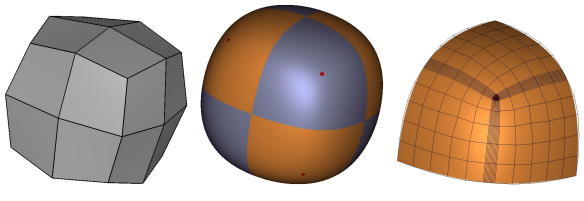

(a) input (b) layout (c) BB-net

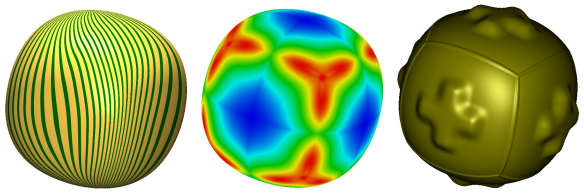

(d) highlight (e) Gauss curvature (f) embossed

Figure 13: High speed single subdivision $\sigma := (\frac{15}{16})$ for $n = 3$.

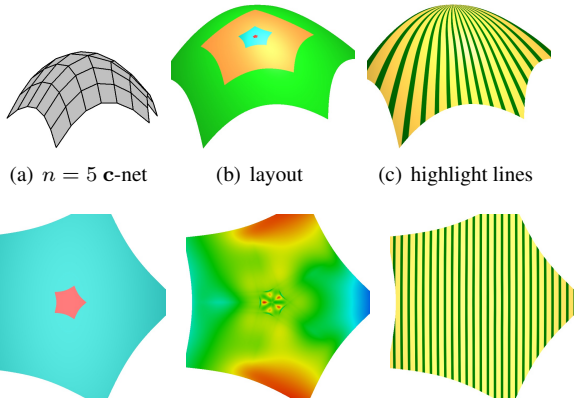

(a) $n = 5$ **c**-net (b) layout (c) highlight lines

(d) zoom to 2nd ring (e) Gauss curvature (f) highlight lines

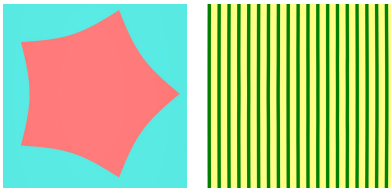

(g) zoom to cap (h) highlight lines

Figure 14: Rapid surface for $\ell = 2$, $\sigma_1 = \frac{3}{4}$, $\sigma_2 = \frac{7}{8}$ with (b) red central cap. Innermost (second) ring $\mathbf{x}^1$ in blue.

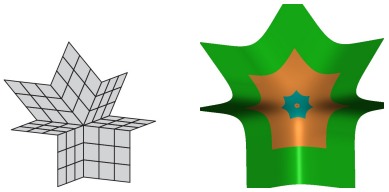

(a) $n = 7$ **c**-net (b) layout

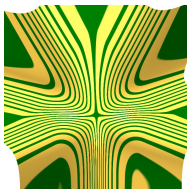

(c) highlight lines

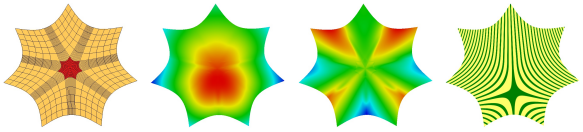

(d) $\mathbf{x}^3$ + cap (e) Gauss (f) Mean (g) highlight lines

Figure 15: Rapid surface for $\ell = 3$, $\sigma := (\frac{3}{4}, \frac{7}{8}, \frac{7}{8})$. (d) BB-net of last ring $\mathbf{x}^3$ plus red central cap, cf. (b). (e,f) Gauss and Mean curvature and highlight lines of this ring and the cap.

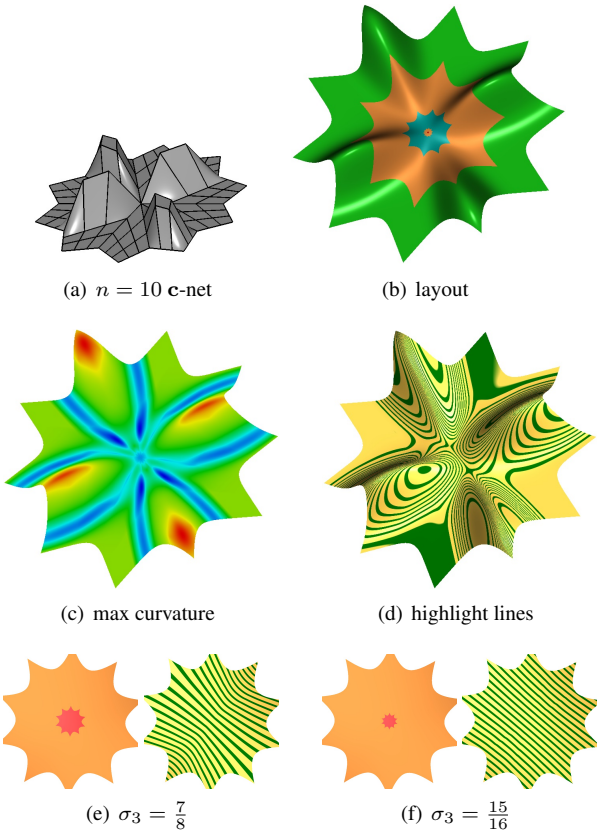

(a) $n = 10$ **c**-net (b) layout

(c) max curvature (d) highlight lines

(e) $\sigma_3 = \frac{7}{8}$ (f) $\sigma_3 = \frac{15}{16}$

Figure 16: Rapid surface for default $\ell = 3$: $\sigma := (\frac{3}{4}, \frac{7}{8}, \frac{7}{8})$ with (b) tiny central red cap. (e,f) compare choices for σ_3.

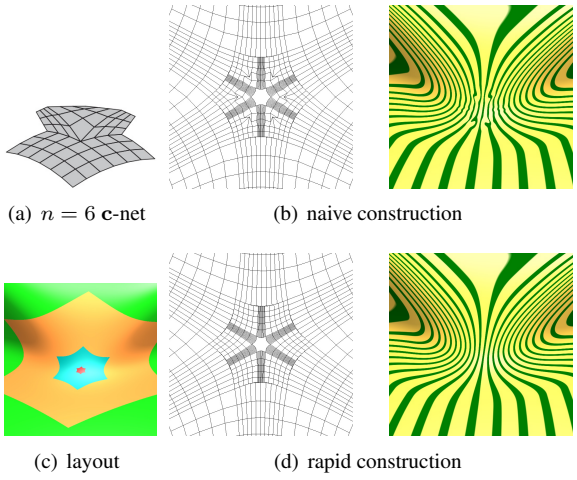

(a) $n = 6$ **c**-net (b) naive construction

(c) layout (d) rapid construction

Figure 17: Rapid surface for $\ell = 2$, $\sigma := (\frac{3}{4}, \frac{7}{8})$ with red central cap. (b,d) BB-net and highlight lines of the (b) the 'naive' and (d) the default rapid construction.

7 Examples and discussion

In the following, when the layout of the polynomial pieces is displayed, the surrounding bi-3 ring is colored green. When $n > 4$, choosing the default

$$\text{speed sequence } \sigma \text{ as } (\sigma_1, \sigma_2, \sigma_3) := (\frac{3}{4}, \frac{7}{8}, \frac{7}{8})$$

yields a central cap smaller than 8 CC-refinements! Setting also $\sigma_1 := \frac{7}{8}$ typically yields good quality but results in minor flaws in some extreme higher valence configurations. Similarly, setting $\sigma_3 := \frac{15}{16}$ yields a slightly worse highlight line distribution, albeit only under the microscope (Fig. 16).

The case $n = 3$ is special: $\sigma := (\frac{15}{16})$ yields high-quality surfaces with a tiny cap, see Fig. 12 and Fig. 13. Fig. 12b,d advertises improved shape of the new construction over Catmull-Clark subdivision for $n = 3$ and Fig. 23 for $n = 6$.

Although the central G^1 cap construction assumes that the cap is so tiny that no more refinements are needed for geometry or analysis (see e.g. Fig. 14b). Nevertheless the shape requirements are high: the central cap should not be noticeable in the highlight line distribution. To see this compare Fig. 24 (a) vs (b). While we can improve the Gauss curvature Fig. 14e by splitting each cap sector as a 2×2 macro patch, we prefer the simpler cap, see Fig. 14c,f,h.

For $n = 7$, Fig. 15 demonstrates the quality of the default choice $\ell = 3$, $\sigma := (\frac{3}{4}, \frac{7}{8}, \frac{7}{8})$. The red central cap does not disrupt the highlight line distribution. Fig. 16 demonstrates that $\sigma_3 := \frac{15}{16}$ can still work even for $n = 10$.

Fig. 17 demonstrates failure when implementing rapid surfaces without the characteristic parameterizations of [10]. For the example, for $n = 6$, we chose $\ell = 2$, $\sigma := (\frac{3}{4}, \frac{7}{8})$ when splitting the tensor-borders $\tilde{\mathbf{t}}^r$, i.e. a consecutive λ^2, λ^3 scaling of the guide $\mathbf{g}$ by deCasteljau, and sampling with $\tilde{\chi}_{\frac{1}{2}}$ of Catmull-Clark subdivision. While the first ring shows only minor flaws, choosing $\sigma_2 = \frac{7}{8}$ for the second ring leads to a disastrous highlight line distribution. As Fig. 17c,d demonstrate, this is not a problem of the geometric data but of the parameterization.

Fig. 18 illustrates why we chose a guide $\mathbf{g}$ of total degree 6 rather than 5. Degree 5 works in most cases, but the 'isolated cliff' input configuration of Fig. 18a results in a noticeable dip for the lower degree option. Note that the degree of the guide is not reflected in the degree of the final surface.

Fig. 19 interogates the structure and quality of the piece of Fig. 1 that was embossed with two patterns.

Fig. 20 shows the that even extreme convergence speed can be a useful design component when the emerging shape flaws are irrelevant because local editing is expected. Fig. 22 shows rapid surfaces in a larger design context. The highlight lines include parts of the regular green neighborhood.

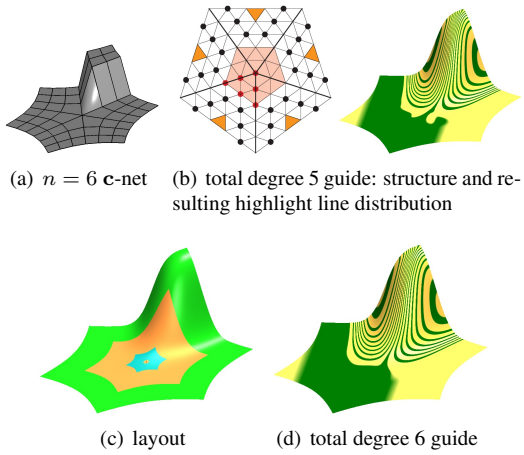

(a) $n = 6$ $\mathbf{c}$-net (b) total degree 5 guide: structure and resulting highlight line distribution

(c) layout (d) total degree 6 guide

Figure 18: Failure of a total degree 5 guide for a challenging $\mathbf{c}$-net.

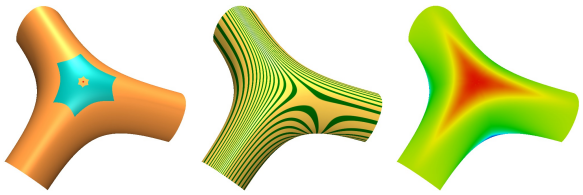

(a) layout (b) highlight lines (c) Gauss curvature

Figure 19: Green part of the dodecahedral surface of Fig. 1.

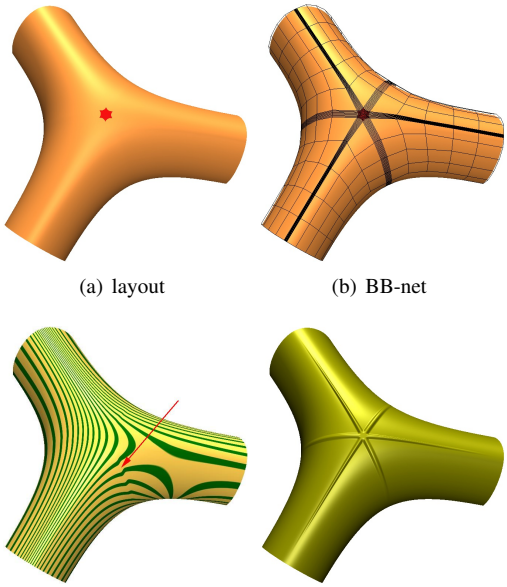

(a) layout (b) BB-net

(c) deficient highlight lines (d) editing

Figure 20: Extreme speed $\sigma := (\frac{31}{32})$, one bi-5 ring + red cap (cf. Fig. 19), resulting in deficient highlight line distribution (c) across the narrow corridor between corner patches (b). The corridor is narrow due to the extremely rapid refinement (a). After editing (lifting the free coefficients in the corridor) this deficiency is irrelevant (d).

8 Conclusion

The idea of rapid subdivision is simple and natural: rapid subdivsion generalizes the split $\sigma : 1 - \sigma$ of the tensor-product case $n = 4$. Compared to Catmull-Clark subdivision with its subdominant eigenvalue λ and $\sigma := \frac{1}{2}$, this analogy predicts a doubling of the contraction speed when $\sigma = \frac{3}{4}$ to approximately λ^2; and a tripling of the speed when $\sigma = \frac{7}{8}$ to approximately λ^3. Rapid subdivision realizes this prediction, also for higher speed σ, by leveraging the characteristic parameterization of adjustable speed subdivision [10], constructing a new piecewise C^1 guide of total degree 6 with a unique cubic expansion at the center point; and by stabilizing the process with a guide surface [6]. Rapid subdivision can stand on its own: it is easy to analyze and guarantees smoothness in the limit. We turn rapid subdivision into a finite construction by completing the otherwise C^2 surface by a tiny central G^1 cap of degree bi-5. Since the tiny cap preserves and prolongs the highlight line distribution of the main surface body, this construction satisfies both shape and refinability requirements of modeling and analysis.

We think it unlikely that equally high surface quality can be achieved by simple averaging formulas of the input net, or without the carefully chosen rapid characteristic parametrizations.

Acknowledgements This work was supported in part by DARPA HR00111720031 and NIH R01 LM011300-01.

References

[1] E. Catmull, J. Clark, Recursively generated B-spline surfaces on arbitrary topological meshes, Computer-Aided Design 10 (1978) 350–355.

[2] D. Doo, M. Sabin, Behaviour of recursive division surfaces near extraordinary points, Computer-Aided Design 10 (1978) 356–360.

[3] U. H. Augsdörfer, N. A. Dodgson, M. A. Sabin, Artifact analysis on b-splines, box-splines and other surfaces defined by quadrilateral polyhedra, Computer Aided Geometric Design 28 (3) (2011) 177–197.

[4] K. Karciauskas, J. Peters, U. Reif, Shape characterization of subdivision surfaces – case studies, Computer Aided Geometric Design 21 (6) (2004) 601–614.

[5] A. Levin, Modified subdivision surfaces with continuous curvature, ACM Trans. Graph 25 (3) (2006) 1035–1040.
URL http://doi.acm.org/10.1145/1141911.1141990

[6] K. Karčiauskas, J. Peters, Concentric tesselation maps and curvature continuous guided surfaces, Computer Aided Geometric Design 24 (2) (2007) 99–111.

[7] E. Akleman, V. Srinivasan, J. Chen, Interactive modeling of smooth manifold meshes with arbitrary topology: G^1 stitched bi-cubic bzier patches, Computer & Graphics, Special Issue on SMI 2017 66 (2017) 64–73.

[8] K. Karčiauskas, J. Peters, A new class of guided C^2 subdivision surfaces combining good shape with nested refinement, Computer Graphics Forum (2017) to appear.

[9] J. Peters, U. Reif, Subdivision Surfaces, Vol. 3 of Geometry and Computing, Springer-Verlag, New York, 2008.

[10] K. Karčiauskas, J. Peters, Adjustable speed surface subdivision, Computer Aided Geometric Design. 26 (2009) 962–969.

[11] K.-P. Beier, Y. Chen, Highlight-line algorithm for realtime surface-quality assessment, Computer-Aided Design 26 (4) (1994) 268–277.

[12] G. Farin, Curves and Surfaces for Computer Aided Geometric Design: A Practical Guide, Academic Press, San Diego, 2002.

[13] H. Prautzsch, W. Boehm, M. Paluszny, Bézier and B-spline techniques, Springer Verlag, 2002.

[14] J. Stam, Exact evaluation of Catmull-Clark subdivision surfaces at arbitrary parameter values, in: Proceedings of the ACM Conference on Computer Graphics (SIGGRAPH-98), ACM Press, New York, 1998, pp. 395–404.

[15] J. Peters, Evaluation and approximate evaluation of the multivariate Bernstein-Bézier form on a regularly partitioned simplex, Transactions of Mathematical Software 20 (4) (1994) 460–480.

Appendix: BB-coefficients of a scaled triangular domain

It is well known that if Bézier curve with BB-coefficients $\mathbf{p}_i$, $i = 0, \ldots, d$ of degree d defined over unit interval $[0..1]$ is restricted to subinterval $[0..\lambda]$, BB-coefficients $\bar{\mathbf{p}}_i$ of restriction can be computed via formula

$$\bar{\mathbf{p}}_i := \sum_{k=0}^{i} B_k^i(\lambda)\mathbf{p}_k \ ,$$

where B_k^i are the Bernstein polynomials. Applying this formula first in one parameter and then in a second yields the BB-coefficients of the restriction to scaled triangular domain (see Fig. 21a,b and [15]).

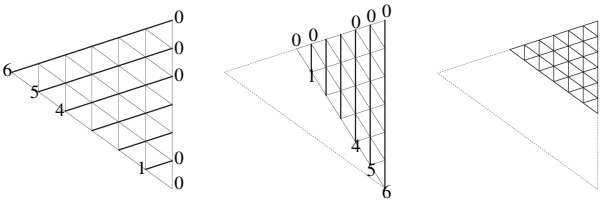

(a) 1st step (b) 2nd step (c) restriction

Figure 21: Domain restriction: $D \to SD$.

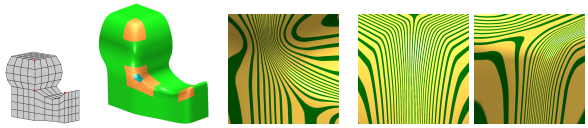

(a) **c**-net (b) layout (c) $n = 5$ (d) $n = 3$

Figure 22: Model of a tow hitch with three rapid subdivision surfaces.

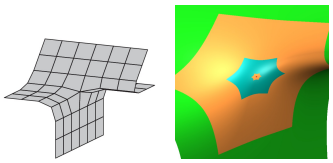

(a) $n = 6$ (b) layout

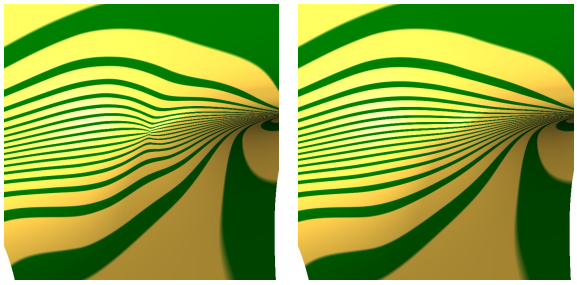

(c) Catmull-Clark subdivision (d) rapid

Figure 23: (c) Pinching in the highlight line distribution in standard Catmull-Clark subdivision. (d) Rapid surface with $\ell = 3$, $\sigma := (\frac{3}{4}, \frac{7}{8}, \frac{7}{8})$.

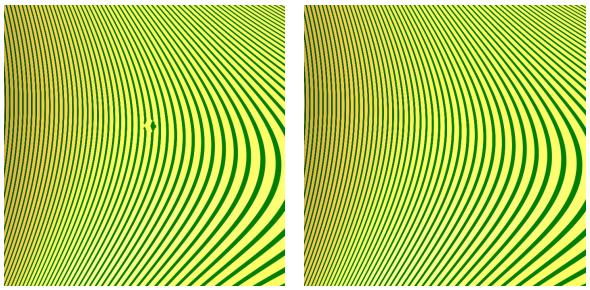

(a) Coons cap (b) G^1 cap

Figure 24: The importance of carefully selecting a high-quality cap. Surface of Fig. 19 zoom in to the last two rings plus cap. (a) C^0-connected $n = 6$ Coons patches interpolating the boundary and straight lines to the center point. The defect in the highlight line distribution is visible even for this very small cap. (b) Cap constructed according to Section 6.